EVALUATING THE RELATIVE CONTRIBUTION OF PHOTOSYSTEMS I AND II FOR LEAF NITROGEN ESTIMATION USING FRACTIONAL DEPTH OF FRAUNHOFER LINES AND SIF DERIVED FROM SUB-NANOMETER AIRBORNE HYPERSPECTRAL IMAGERY

A. Belwalkar[1], T. Poblete[1,2], A. Hornero[1,3], P.J. Zarco-Tejada[1,2,3]

[1]Department of Infrastructure Engineering, Faculty of Engineering and Information Technology (FEIT), The University of Melbourne, Melbourne, Victoria, Australia
[2]School of Agriculture, Food and Ecosystem Sciences (SAFES), Faculty of Science (FoS), The University of Melbourne, Melbourne, Victoria, Australia
[3]Instituto de Agricultura Sostenible (IAS), Consejo Superior de Investigaciones Científicas (CSIC), Alameda del Obispo s/n, 14004 Córdoba, Spain

ABSTRACT

Integrating far-red solar-induced chlorophyll fluorescence (SIF_{760}) and leaf biochemical constituents (primarily leaf chlorophyll content (C_{a+b})) has recently been demonstrated to improve the estimation of leaf nitrogen (N) concentration from airborne and spaceborne hyperspectral imagery in homogenous and heterogeneous crop canopies. The advent of sub-nanometer resolution imagers capable of detecting narrow solar Fraunhofer lines (FLs) has enabled a novel opportunity to investigate the prospect of leaf N estimation using individual FLs in addition to SIF_{760} and C_{a+b} traits. This study seeks to determine whether incorporating distinct FL depth derived from sub-nanometer airborne hyperspectral imagery could improve leaf N estimates. A sub-nanometer hyperspectral imager with ≤0.2 nm full-width at half-maximum (FWHM) resolution was flown in tandem with a narrow-band hyperspectral imager with 5.8 nm FWHM over a winter wheat field. Plots were fertilized with variable concentrations of nitrogen to enable nutrient variability. Regression models utilizing Gaussian process regression (GPR) were built with different permutations of SIF, C_{a+b} and depths of individual FLs for estimating leaf N concentration. Laboratory-determined leaf N estimates were obtained by destructive sampling. Results show that GPR models incorporating the depth of distinct Fraunhofer lines as predictor variables performed better than the benchmark model constructed using C_{a+b} and SIF_{760} alone. The best leaf N-estimation model built with FLs from the red and far-red regions (C_{a+b}, $FL_{682.97\ nm}$, $FL_{757.002\ nm}$) yielded an R^2 of 0.71, outperforming the standard approach used in previous works (C_{a+b}, SIF_{760}) ($R^2 = 0.56$).

Index Terms— Airborne, Hyperspectral, SIF, GPR, leaf Nitrogen, Fraunhofer lines, sub-nanometer

1. INTRODUCTION

Nitrogen is a macronutrient that plays a crucial role in plant development, yield and grain quality, whilst it is often the dominant limiting factor in photosynthesis [1], [2]. Accurate field-wide assessments of leaf N concentration (N%) enable more targeted use of N-fertilizers, thereby mitigating the environmental effects of N-overfertilization while improving crop yields. Standard destructive sampling for leaf N determination relies on the laboratory analysis of leaf tissue using methods such as Kjeldahl digestion and Dumas combustion. Although accurate, these techniques are time-consuming and expensive for monitoring the leaf N status of large areas. In recent decades, the use of remote sensing technologies has increased, particularly through hyperspectral imagery, for mapping the spatial and temporal variations of crop leaf N concentration at the paddock scale [3]. There are three main categories of leaf N estimation approaches: 1) empirical methods, 2) physically-based model inversion methods, and 3) hybrid regression methods. Among these approaches, hybrid regression methods integrate physically-based models with advanced machine learning (ML) algorithms taking advantage of both the physical basis provided by radiative transfer models (RTMs) and the adaptability and efficiency of ML methods [4].

Recent studies utilizing narrow-band airborne and spaceborne hyperspectral imagers have demonstrated that accurate determination of leaf N concentration is feasible by combining the RTM-derived leaf biochemical constituents with SIF_{760} acquired from high-resolution airborne hyperspectral imagery [5]–[7]. Even though these studies have demonstrated improved leaf N retrievals when including SIF_{760}, the potential of other spectral regions within the 650-800 nm SIF emission region to characterize both PSI and PSII photosystems has not yet been explored. Moreover, the potential information extracted from the red spectral region, i.e. SIF quantified at the O_2-B absorption

IGARSS 2023 - 2023 IEEE International Geoscience and Remote Sensing Symposium | 979-8-3503-2010-7/23/$31.00 ©2023 IEEE | DOI: 10.1109/IGARSS52108.2023.10281680

band centered around 687 nm (SIF_{687}) and the depth of solar FLs, which are absorption lines in the solar spectrum, could provide valuable insights for improved characterization of photosynthesis and leaf N variability. With the recently developed sub-nanometer resolution airborne hyperspectral imagers, it is now possible to investigate the potential of these narrow FLs within the SIF emission region. This study aims to assess the relative contribution of the solar-induced chlorophyll fluorescence emitted by each of the two photosystems (PSI and PSII) in explaining leaf N variability across the field. SIF_{760}, SIF_{687} and the fractional depth of distinct solar FLs inside PSI and PSII emission regions derived from sub-nanometer airborne hyperspectral imagery are evaluated.

2. MATERIALS AND METHODS

2.1. Study site and airborne hyperspectral imagery

An airborne campaign operated by the HyperSens Laboratory at the University of Melbourne's Airborne Remote Sensing Facility was conducted on 9 October 2019 over a phenotyping trial site in Yarrawonga (36°02′55"S, 145°59′02"E), Australia. Several cultivated varieties of rainfed wheat were grown under varying physiological conditions and N fertilization treatments. A sub-nanometer hyperspectral imager (FWHM ≤0.2 nm; 670–780 nm) and a narrow-band hyperspectral imager (FWHM = 5.8 nm; 400–1000 nm) (Headwall Photonics Inc., Fitchburg, MA, USA) were used to collect airborne hyperspectral imagery at 20 cm spatial resolution. Concurrent with the flights, ground measurements were conducted using a CC-3 VIS-NIR cosine corrector diffuser attached to an HR-2000 spectrometer (Ocean Insight, Dunedin, FL, USA) with a 0.065-nm FWHM for continuous measurement of the total incident radiation at the trial site. Pure vegetation pixels were extracted within individual plots, and mean radiance spectra corresponding to the sub-nanometer imager and reflectance spectra from the narrow-band hyperspectral imager were retrieved. Belwalkar *et al.* [8] provide a full description of the airborne campaign, data preprocessing, and image correction. In addition, the total leaf N concentration (%) was destructively determined in the laboratory using the Kjeldahl method, with samples consisting of 10–15 leaves randomly selected per plot.

2.2. SIF quantification and identification of Fraunhofer lines

The irradiance spectra obtained from the HR-2000 spectrometer were convolved to the spectral characteristics of the sub-nanometer imager using Gaussian convolution. Using this convolved irradiance and the mean radiance derived from each plot, SIF_{760} and SIF_{687} were quantified using the *in-filling* approach, employing the Fraunhofer Line Depth (FLD) principle with a total of three spectral bands (3FLD) [9]. Furthermore, we identified 17 FLs across the 670–780 nm spectral range of the sub-nanometer imager, excluding regions of significant water vapour and oxygen absorption [10]. The identified FLs were divided into two groups according to their positions in the spectral region. Five of these FLs were located in the red region of the spectrum (named here as red FLs), while the remaining twelve were located within the far-red region (named here as far-red FLs). The exact location of the band centres corresponding to all FLs, and the O_2-A and O_2-B oxygen absorption bands is illustrated in Fig. 1. For each FL, the absolute depth in radiance units was computed as the difference between the radiance at the left shoulder wavelength and the wavelength at the bottom of the FL. The left shoulder wavelength was selected by searching for the local maxima closest to the bottom FL wavelength within 1 nm.

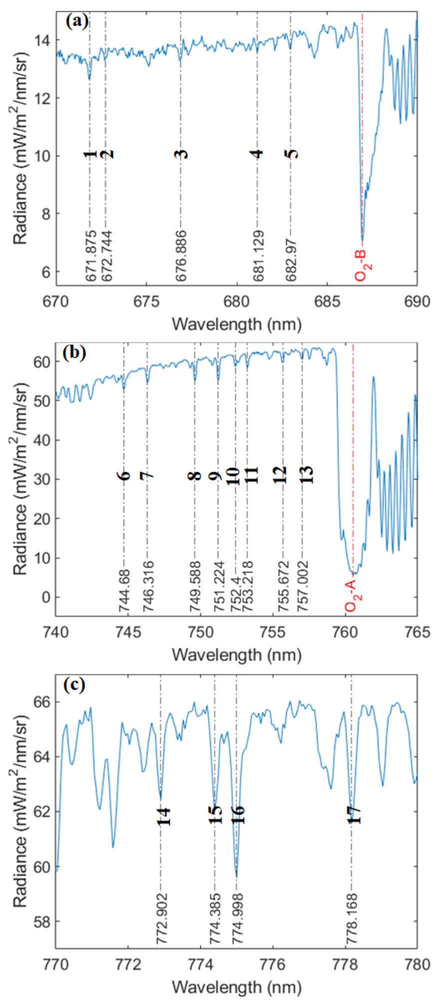

Fig. 1: Locations of the band centres corresponding to red FLs (a) and far-red FLs (b,c) shown in dashed black, and oxygen absorption lines (a,b) shown in dashed red identified from the average radiance spectra of one of the plots imaged by the sub-nanometer hyperspectral imager.

2.3. Regression model for N concentration estimation

We trained regression models based on GPR to empirically estimate leaf N concentration using C_{a+b}, SIF_{760}, SIF_{687} and the depth of distinct FLs as a pool of potential predictor variables. C_{a+b}, SIF_{760}, and depth corresponding to a single FL were used to initially train GPR models. Subsequently, GPR models were trained using C_{a+b}, and one FL depth each from the red and far-red FL groups on leaf N estimation to further examine the effect of using FL depths corresponding to both the red and far-red FL groups as predictor variables. The GPR models were trained in parallel (MATLAB parallel computing toolbox), and the hyperparameters were optimized by incorporating Bayesian optimization into the leave-one-out cross-validation (LOOCV). The performance evaluation of the trained GPR models was carried out using the coefficient of determination (R^2), root-mean-square error (RMSE) and normalized root-mean-square error (nRMSE). To limit random errors, for each possible combination of predictor variables, five GPR models were independently trained, and the average estimate was then used to determine R^2, RMSE and nRMSE.

Soil-Canopy Observation of Photosynthesis and Energy (SCOPE) [11] RTM-based hybrid inversion with random forest regression [12] was used to estimate C_{a+b} from the mean reflectance spectra obtained from the narrow-band hyperspectral imager in the 400-800 nm spectral region. To determine if the leaf N estimates could be further improved by including SIF emission regions other than the O_2-A absorption band, we used the GPR model developed with C_{a+b} and SIF_{760} as a benchmark. Then, we compared this benchmark by adding the depth of distinct solar FLs into the models. Since PSII largely influences the red spectral region, the contributions of SIF_{687} and red FLs would be attributed only to PSII. In contrast, the contributions of SIF_{760} and far-red FLs would be attributed to both photosystems.

3. RESULTS

GPR models trained with a single FL as one of the three predictor variables produced a total of 17 distinct GPR models (5 models for the red FL group and 12 models for the far-red FL group). Among the red FL group, the performance of the GPR model with FL_1 depth was comparable with the benchmark (R^2 = 0.56; RMSE = 0.229%; nRMSE = 5.89%; Fig. 2a and 2b), whereas the performance of the other four red FL depths did not improve the prediction. From the far-red FLs, the model that included FL_{13} depth showed the highest performance, outperforming the benchmark model (R^2 = 0.63; RMSE = 0.21%; nRMSE = 5.41%; Fig. 2c). Since FL_{13} performed the best among all red and far-red FLs, for the next set of GPR models with two FLs and C_{a+b} as predictors, we selected FL_{13} among the far-red FLs and independently evaluated all five red FLs as potential GPR model predictors. When compared to the benchmark model, the GPR model trained with FL_5 (682.97 nm) and FL_{13} (757.002 nm) substantially improved the leaf N estimation (R^2 = 0.71; RMSE = 0.188%; nRMSE = 4.84%; Fig. 2d) with more data points closer to the 1:1 line. The model's performance did not improve further after including more FLs from either of the two FL groups. Furthermore, we found that the model's performance decreased by including SIF_{687} with any combination of predictor variables. This result could be potentially attributed to the high collinearity observed between C_{a+b} and SIF_{687}.

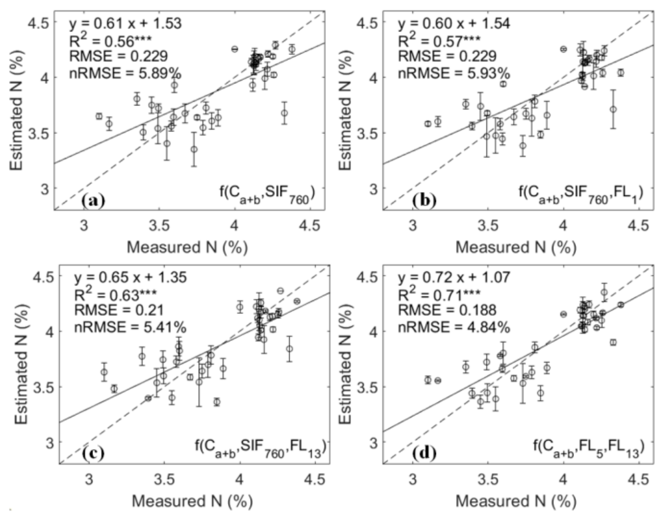

Fig. 2: Measured vs estimated mean leaf N concentration using the best GPR models as a function of C_{a+b} and SIF_{760} (a), C_{a+b}, SIF_{760} and best performing red FL (b), C_{a+b}, SIF_{760} and best performing far-red FL (c), C_{a+b} and best-performing combination of one red and one far-red FL (d). The dashed line indicates the 1:1 line. The error bars indicate the standard deviation based on five runs of the GPR model. The GPR model as a function of C_{a+b} and SIF_{760} was used as a benchmark. ****p*-value<0.05.

Our results suggest that FL depths corresponding to 757.002 nm (FL_{13}) and 682.97 nm (FL_5), in conjunction with C_{a+b} estimated by RTM simulations, provided improved estimates of leaf N concentration. These results provide a foundation for future research into the use of FLs identified in sub-nanometer imagery in the context of precision agriculture and plant physiology monitoring. Future work will focus on evaluating their potential for identifying pre-visual signs of vegetation stress.

4. CONCLUSIONS

This study evaluated the capability of 17 narrow solar Fraunhofer lines depth derived from sub-nanometer imagery to estimate leaf N concentration when combined with C_{a+b} and SIF_{760}. With an RMSE of less than 0.19%, the best results were achieved by the regression model constructed using C_{a+b}, red FL closest to O_2-B band (682.97 nm), and far-red FL closest to O_2-A band (757.002 nm). These results highlight the importance of integrating FLs around the two oxygen absorption bands for more accurate leaf N estimates. Furthermore, the proposed approach based on the depth of distinct FLs demonstrates the importance of sub-nanometer resolution imaging sensors for vegetation trait retrievals, supporting the need for future research focused on the entire SIF emission region for physiological assessment and vegetation stress detection.

5. ACKNOWLEDGEMENTS

The Foundation for Arable Research Australia and Riverine Plains Incorporated provided and managed the plot trials, which the authors gratefully acknowledge. We thank A. Gracia-Romero and A. Longmire for their technical support during the field and airborne campaign.

6. REFERENCES

[1] J. R. Evans, "Photosynthesis and nitrogen relationships in leaves of C3 plants," Oecologia, vol. 78, no. 1, pp. 9–19, 1989.

[2] G. Lemaire, M. H. Jeuffroy, and F. Gastal, "Diagnosis tool for plant and crop N status in vegetative stage: Theory and practices for crop N management," European Journal of Agronomy, vol. 28, no. 4, pp. 614–624, May 2008.

[3] K. Berger et al., "Crop nitrogen monitoring: Recent progress and principal developments in the context of imaging spectroscopy missions," Remote Sensing of Environment, vol. 242, June 2020.

[4] J. Verrelst et al., "Quantifying Vegetation Biophysical Variables from Imaging Spectroscopy Data: A Review on Retrieval Methods," Surveys in Geophysics, vol. 40, no. 3, pp. 589–629, May 2019.

[5] Y. Wang, L. Suarez, T. Poblete, V. Gonzalez-Dugo, D. Ryu, and P. J. Zarco-Tejada, "Evaluating the role of solar-induced fluorescence (SIF) and plant physiological traits for leaf nitrogen assessment in almond using airborne hyperspectral imagery," Remote Sensing of Environment, vol. 279, Sep. 2022.

[6] Y. Wang, L. Suarez, V. Gonzalez-Dugo, D. Ryu, P. Moar and P. J. Zarco-Tejada, "Leaf nitrogen assessment with ISS DESIS Imaging Spectrometer as compared to high-resolution airborne hyperspectral imagery," in IEEE International Geoscience and Remote Sensing Symposium, Kuala Lumpur, Malaysia, pp. 5444–5447, 17–22 July 2022.

[7] C. Camino, V. González-Dugo, P. Hernández, J. C. Sillero, and P. J. Zarco-Tejada, "Improved nitrogen retrievals with airborne-derived fluorescence and plant traits quantified from VNIR-SWIR hyperspectral imagery in the context of precision agriculture," International Journal of Applied Earth Observation and Geoinformation, vol. 70, pp. 105–117, Aug. 2018.

[8] A. Belwalkar, T. Poblete, A. Longmire, A. Hornero, R. Hernandez-Clemente, and P. J. Zarco-Tejada, "Evaluation of SIF retrievals from narrow-band and sub-nanometer airborne hyperspectral imagers flown in tandem: Modelling and validation in the context of plant phenotyping," Remote Sensing of Environment, vol. 273, May 2022.

[9] S. W. Maier, K. P. Gunther, and M. Stellmes, "Sun-Induced Fluorescence: A New Tool for Precision Farming," In: Digital Imaging and Spectral Techniques: Applications to Precision Agriculture and Crop Physiology, Vol. 66 (eds M McDonald, J Schepers, L Tartly, T Van Toai, D Major), ASA Spec. Publ., Madison, WI, USA, pp. 209– 222, 2003.

[10] L. P. Albert, K. C. Cushman, Y. Zong, D. W. Allen, L. Alonso, and J. R. Kellner, "Sensitivity of solar-induced fluorescence to spectral stray light in high resolution imaging spectroscopy," Remote Sensing of Environment, vol. 285, Feb. 2023.

[11] C. van der Tol, W. Verhoef, J. Timmermans, A. Verhoef, and Z. Su, "An integrated model of soil-canopy spectral radiances, photosynthesis, fluorescence, temperature and energy balance," Biogeosciences, vol. 6, pp. 3109–3129, 2009.

[12] A. Belwalkar, T. Poblete, A. Hornero, and P. J. Zarco-Tejada, "Accounting for the spectral resolution on SIF retrieval from a narrow-band airborne imager using SCOPE," in IEEE International Geoscience and Remote Sensing Symposium, Kuala Lumpur, Malaysia, pp. 5440–5443, 17–22 July 2022.